Electromagnetic diffraction analysis of columned grid gratings

2002 J. Opt. A: Pure Appl. Opt. 4 180

(http://iopscience.iop.org/1464-4258/4/2/310)

INSTITUTE OF PHYSICS PUBLISHING JOURNAL OF OPTICS A: PURE AND APPLIED OPTICS
J. Opt. A: Pure Appl. Opt. **4** (2002) 180–186 PII: S1464-4258(02)28628-6

Electromagnetic diffraction analysis of columned grid gratings

Dianwen Zhang, Zhenwu Lu, Weixing Yu and Fengyou Li

State Key Lab of Applied Optics, Changchun Institute of Optics, Fine Mechanics and Physics
Chinese Academy of Sciences, PO Box 1024, Changchun 130022,
People's Republic of China

Received 17 May 2001, in final form 29 October 2001
Published 4 February 2002
Online at stacks.iop.org/JOptA/4/180

Abstract
Binary optics processing methods may be applied to a glass or silicon substrate to generate an array of small columns in order to enhance transmission. We employ the rigorous vector coupled-wave theory to analyse the electromagnetic diffraction nature of two-dimensional columned grid gratings. By computer simulation and calculation, the relation between the reflectivity and the structure parameters of such gratings is presented. These results show that a glass grating can achieve antireflection over almost the whole visible light waveband for unpolarized light, while a silicon grating with a columned grid substrate can achieve low reflectance over as broad a field of view as a tapered silicon grating structure, but it can be fabricated more simply.

Keywords: Columned grating, coupled-wave analysis, antireflection, diffractive optics

(Some figures in this article are in colour only in the electronic version)

1. Introduction

It is well known that conventional methods of producing extremely antireflective surfaces are limited, because of the limited number of thin-film coating materials available for use today in the infrared region. Experimental and theoretical studies show that subwavelength surface-relief gratings exhibit antireflective properties. Such antireflection surfaces can be fabricated by etching a surface-relief structure, i.e. a cuboid grid or columned grid, upon a substrate. It is important that we obtain fuller details of the parameters of such structures by a theoretical analysis.

To study the diffraction characteristics of structures which have a feature size comparable to the wavelength of light, rigorous diffraction theories are required. The coupled-wave approach has attracted wide interest because of its easier mathematical solution. Bräuer and Bryngdahl described the coupled-wave method in computing the diffraction efficiencies for two-dimensional (2D) crossed gratings [1]. Vincent applied a finite-difference method to analyse a 2D pyramidal grating [2]. Han *et al* published a study of the electromagnetic scattering of a dielectric sinusoidal grating [3], in which the coupled-wave calculation results were compared with those from the graded-index model which was used in [4–13].

To our knowledge, there has been no theoretical discussion on columned grid gratings with spatial periods and groove depths comparable to the incident wavelength. We have found, by computer simulation, that this kind of grating has better antireflection properties than rectangular grid gratings. Additionally, these structures are also favourable for the fabrication and replication of diffractive elements in the far-infrared waveband.

The crucial point of the coupled-wave theory is to treat the electromagnetic field within the grating region. In this paper, the permittivity of the grating region is represented by means of a Fourier expansion, as in the method of Knop [14]. Then we use the new formulation presented by Li [15] to displace the old formulation published by Knop, which may further improve the convergence of this algorithm in the calculation. In fact, it has been shown that the field solutions to the coupled-wave equations do indeed verify energy conservation [16]. In this calculation, it is proved that the sum of the reflectivity and transmittance of waves of all orders is approximatively equal to 1. It can also be shown that, regardless of the number of waves included in the coupled-wave analysis, this condition is always satisfied [7].

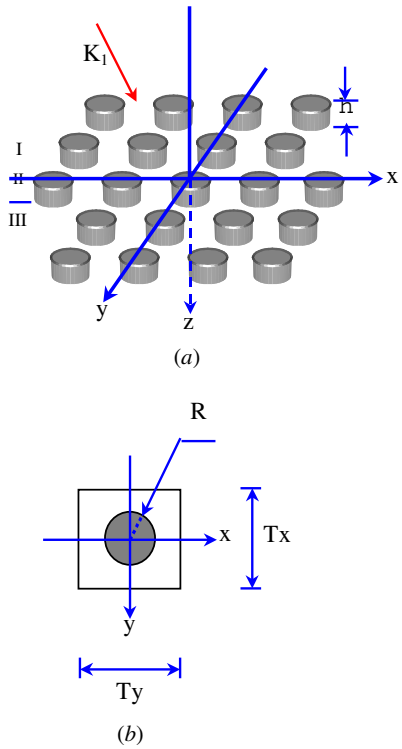

Figure 1. Coordinate geometry (a) and platform (b) of a wave incident on a 2D columned grid grating.

The organization of the reminder of this paper is as follows. The columned grid grating problem is defined in section 2, which introduces the geometry and notation used. In section 3, we review the rigorous coupled-wave analysis and describe the numerical solution. Section 4 presents the computer simulation results, and section 5 contains a summary and conclusion of the work.

2. Description of the geometry and notation

The geometry and notation of the problem presented here are similar to those of Bräuer and Bryngdahl [1], and Han *et al* [3]. We consider the coordinate geometry of the problem shown in figures 1 and 2. The structure of the grating with an array of columns is divided into three regions. In figure 1(a), region I extends infinitely into the incident half-space from the surface of the grating. We assume the medium in this region is isotropic and its permittivity is ε_{I}. Region II is a periodic surface-relief structure consisting of the materials of regions I and III. In this region, the height h of the array of columns is defined to be the depth of the grating structure. It extends from the tops of the surface peaks to the bottoms of the valleys around the columns. The parameters of the surface profile of the periodic structure are defined in figure 1(b). The profile of interest is periodic in two dimensions. The grating is of period T_x along the x direction and T_y along the y direction.

As shown in figure 2, the incident plane is defined as the plane containing the $\boldsymbol{k}_1$ vector and the normal to the grating surface that is the z-axis. The $\boldsymbol{k}_1$ vector makes an angle α with the z-axis, and we assume that the electric field is polarized at an angle ψ to the incident plane. Region III extends from the bottoms of the columns into the transmission half-space.

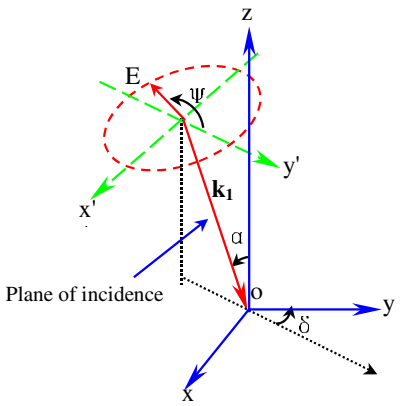

Figure 2. Definition of the incidence angles a, δ and the polarization angle Ψ. The electric field vector $\boldsymbol{E}$ of the incident wave is in the plane perpendicular to $\boldsymbol{k}$ and y' is parallel to the y-axis; $\boldsymbol{E}$ and y' determine Ψ.

It contains a homogeneous medium of permittivity $\varepsilon_{\mathrm{III}}$. The wavevector magnitudes in regions I and III are $k = k_0\sqrt{\varepsilon_{\mathrm{I}}}$ and $k_3 = k_0\sqrt{\varepsilon_{\mathrm{III}}}$, respectively, where $k_0 = 2\pi/\lambda_0$ and λ_0 is the free-space wavelength. We denote the unit vectors along the x, y and z axes as $\boldsymbol{i}$, $\boldsymbol{j}$, and $\boldsymbol{k}$, respectively. Within the given geometry in figure 1(a), the wavevector $\boldsymbol{k}_1$ and polarization vector $\boldsymbol{u}$ can be given.

In figure 1(a) for the grating and incident wave geometry, we assume that all the regions have a free-space magnetic permeability $\mu_0 = 1$ and the grating has finite conductivity so that we can neglect all the surface currents. The permittivity $\varepsilon_{\mathrm{III}}$ is taken to be complex to account for possible material losses.

3. Theoretical analysis

The formulation presented in this section is closest to that of Moharam and Gaylord [17], in which a volume holographic grating was analysed. For convenience, we follow the notation used in their paper.

In regions I and III, the light field may be written in terms of plane-wave expansions. Let $\boldsymbol{E}^{\mathrm{i}}$ be the incident field with wavevector $\boldsymbol{k}_1$ and polarization vector $\boldsymbol{u}$, R_{mn} be the reflected waves with wavevector $\boldsymbol{k}_{1mn}$ in region I and T_{mn} be the transmitted waves with wavevector $\boldsymbol{k}_{3mn}$ in region III, respectively. According to the Rayleigh expansions, the electric fields may thus be represented by

$$E^{\mathrm{I}} = E^{\mathrm{i}} + \sum_{m=-\infty}^{\infty}\sum_{n=-\infty}^{\infty} R_{mn}\exp(\mathrm{i}k_{1mn}r), \qquad (1)$$

$$E^{\mathrm{III}} = \sum_{m=-\infty}^{\infty}\sum_{n=-\infty}^{\infty} T_{mn}\exp[\mathrm{i}k_{3mn}(r-h)]. \qquad (2)$$

In region II, let $\boldsymbol{E}^{\mathrm{II}}$ and $\boldsymbol{H}^{\mathrm{II}}$ be the electric and magnetic fields, respectively. Their components can each be written as an expansion in terms of a particular set of the space harmonics,

which are approximated to be independent of z as follows:

$$E^{\mathrm{II}} = \sum_{m=-\infty}^{\infty} \sum_{n=-\infty}^{\infty} [E_{mn}^{x}(z)i + E_{mn}^{y}(z)j] \exp[\mathrm{i}(k_{xm}i + k_{yn}j)] \tag{3}$$

and

$$H^{\mathrm{II}} = \left(\frac{\varepsilon_0}{\mu_0}\right)^{-\frac{1}{2}} \sum_{m=-\infty}^{\infty} \sum_{n=-\infty}^{\infty} [H_{mn}^{x}(z)i + H_{mn}^{y}(z)j] \times \exp[\mathrm{i}(k_{xm}i + k_{yn}j)]. \tag{4}$$

We want to determine the unknown complex amplitudes R_{mn} and T_{mn} of the diffracted waves by solving the Maxwell equations in region II and matching the electromagnetic boundary conditions at the interface of the three regions. To solve the electric and magnetic fields in region II, Moharam and Gaylord used a state-variable method, which gives the solution in terms of the eigenvalues and eigenvectors of the corresponding coefficient matrix [17] as follows:

$$E_{mm}^{x} = \sum_{j} C_j \omega_{mn,j}^{1} \exp(\lambda_j z) \tag{5}$$

$$E_{mm}^{y} = \sum_{j} C_j \omega_{mn,j}^{2} \exp(\lambda_j z) \tag{6}$$

$$E_{mm}^{x} = \sum_{j} C_j \omega_{mn,j}^{3} \exp(\lambda_j z) \tag{7}$$

$$E_{mm}^{y} = \sum_{j} C_j \omega_{mn,j}^{4} \exp(\lambda_j z) \tag{8}$$

with the eigenvalues λ_j and elements $\omega_{mn,j}^{l}$ of the eigenvector matrix. By substituting equations (5)–(8) into the group of Maxwell's difference equations, we obtain the following characteristic equation:

$$\lambda\omega = A\omega \tag{9}$$

where A is a constant matrix. After determination of the matrix A, we find λ_j and $\omega_{mn,j}^{l}$ by solving the eigenvalues and eigenvectors of A. As in the analysis of Maharam and Gaylord, the solution of the coupled-wave theory involves four main steps:

(1) Calculation of a constant coefficient matrix and corresponding inverse, which are the coefficients of the Fourier expansions of the permittivity and its reciprocal, respectively. In the following, we rewrite ϵ and ϵ^{-1} in the Fourier expansion

$$\epsilon(x,\ y,\ z) = \sum_{p=-\infty}^{\infty} \sum_{q=-\infty}^{\infty} \epsilon_{pq}(z) \exp\left[\mathrm{i}\left(p\frac{2\pi}{T_x}x + q\frac{2\pi}{T_y}y\right)\right] \tag{10}$$

and

$$\epsilon^{-1}(x,\ y,\ z) = \sum_{p=-\infty}^{\infty} \sum_{q=-\infty}^{\infty} \epsilon_{pq}(z) \exp\left[\mathrm{i}\left(p\frac{2\pi}{T_x}x + q\frac{2\pi}{T_y}y\right)\right]. \tag{11}$$

In the calculation, an important point is to determine the coefficient matrix of the Fourier expansions of the permittivity and its reciprocal for the specific problem. For the columned grid grating, the permittivity is expressed as follows:

$$\epsilon = \begin{cases} \epsilon_1 - T_x/2 < x < T_x/2, \ -T_y/2 < y < T_y < T_y/2, \\ \text{and } x^2 + y^2 > (R/2)^2 \\ \epsilon_2 \qquad\qquad x^2 + y^2 < (R/2)^2. \end{cases} \tag{12}$$

The elements of the coefficient matrix of the Fourier expansions of the permittivity are written as follows:

$$\epsilon_{pq}(z) = \begin{cases} e_1 + \pi(e_2 - e_1)\frac{R^2}{4T_x T_y}, & \rho = 0 \\ \frac{R(e_3 - e_1)\cdot J_1(\pi R\rho)}{2\rho T_x T_y} & \rho \neq 0 \end{cases} \tag{13}$$

$$\overline{\epsilon}_{pq}(z) = \begin{cases} e_1^{-1} + \pi(e_2^{-1} - e_1^{-1})\frac{R^2}{4T_x T_y}, & \rho = 0 \\ \frac{R(e_3^{-1} - e_1^{-1})\cdot J_1(\pi R\rho)}{2\rho T_x T_y}, & \rho \neq 0 \end{cases} \tag{14}$$

where $J_1(2\pi r\rho)$ is the Bessel function of the first kind and ρ is equal to $[(p/T_x)^2 + (q/T_y)^2]^{1/2}$. If it is difficult to obtain the mathematical expressions of the integrals for a grating with an irregular profile in a period, we implement the computation in a very efficient way by using a Newton–Simpson double integral algorithm. The computation is very fast and flexible using C++ language, and can perform the calculation for a diversified profile.

(2) Calculation of the eigenvalues λ_j and eigenvectors $\omega_{mn,j}^{l}$ of the constant coefficient matrix A that characterizes the diffracted wave propagation and coupling in region II.

(3) Solution of a linear system deduced from the boundary matching conditions. We consider the electromagnetic boundary conditions and calculate the constant field expansion coefficient C_j left as unknown in equations (5)–(8).

As in the recent study presented by Li, we use the inverse of the Toeplitz matrix generated by the Fourier coefficients $\overline{\epsilon}_{pq}$ and ϵ_{pq} instead of ϵ_{pq} and $\overline{\epsilon}_{pq}$ in steps (2) and (3), respectively, because from the physics we know that the product of the permittivity and the electric field component must be continuous while the permittivity ϵ is discontinuous at the edge of a column, so ϵ and E must together have two pairs of complementary jumps there. The same arrangement is also given to the product of the permittivity and the magnetic components in our programs. This method improves the convergence of the coupled-wave method even more.

(4) The last step of the procedure is to determine the components of R_{mn} and T_{mn}. They are calculated via equations (5)–(8) and the electromagnetic boundary conditions.

The diffraction efficiencies η_{mn}^{I} and η_{mn}^{III} for the reflected and transmitted waves may be given by

$$\eta_{mn}^{1} = \mathrm{Re}(k_{zmn}^{1}/k_{z00}^{1})|R_{mn}|^2 \tag{15}$$

and

$$\eta_{mn}^{\mathrm{III}} = \mathrm{Re}(k_{z\mathrm{mn}}^{\mathrm{III}}k_{z00}^{\mathrm{III}})|T_{mn}|^2 \tag{16}$$

where Re denotes the real part of a variable, and k_{zmn}^{I} and k_{zmn}^{III} are the components along the z-direction of the wavevectors $\boldsymbol{k}_{1mn}$ and $\boldsymbol{k}_{3mn}$, respectively. For a lossless grating in which the permittivity ϵ_{III} is a real number, conservation of energy requires that

$$\sum_{m=-\infty}^{\infty} \sum_{n=-\infty}^{\infty} (\eta_{mn}^{1} + \eta_{mn}^{\mathrm{III}}) = 1. \tag{17}$$

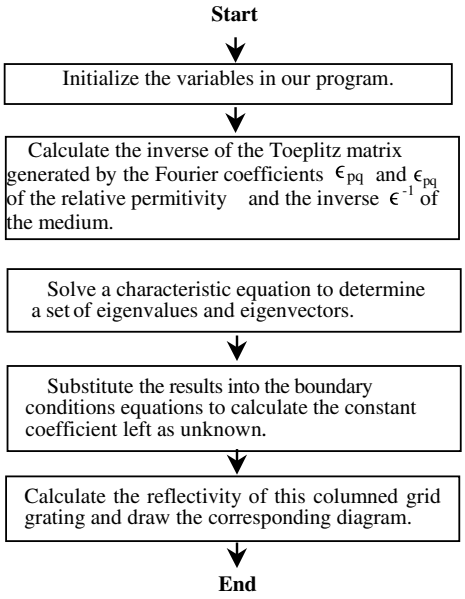

Figure 3. Flow chart of our program.

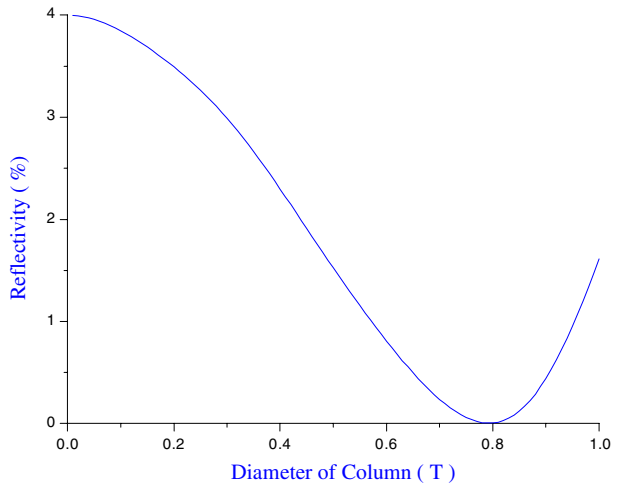

Figure 4. Relation between reflectivity and column diameter for a glass substrate, with parameters: $T = 0.1\lambda$ $h = 0.2\lambda$; $\Psi = 90^\circ$; $\alpha = \delta = 0^\circ$; $n_i = 1.0$; $n_s = 1.5$.

In the calculation, the indices m, n, p and q have to be truncated. The energy conservation condition is necessary but not sufficient for the success of the algorithm, because of losses in the material and the neglect of certain terms in the space harmonics series in the calculation. It can be shown that we must retain a proper number of spatial harmonics (orders) in the analysis to achieve accurate results.

For these calculations Matlab software tool was used, as it is more efficient for dealing with matrices.

4. Numerical results and analysis

We used a standard personal computer with a 800 MHz Pentium III processor and 256 Mbyte memory. The programs were written with Matlab V6.0 and Visual C++ V6.0. In all of our programs, Visual C++ codes were used to calculate the inverse of the Toeplitz matrix generated by the Fourier coefficients $\overline{\epsilon}_{pq}$ and ϵ_{pq} of the relative permittivity ϵ and the inverse ϵ^{-1} of the medium, while Matlab was used to solve Maxwell's differential equations to determine the eigenvalues λ_j, each element $\omega_{mm,j}$ of the eigenvector matrix and the coefficients C_j. Finally we determined the reflectivity of the columned grid grating with a specific structure and used Matlab to plot diagrams of reflectivity versus certain structural parameters. In figure 3, we show the flow chart of all our programs.

We have already mentioned that the spatial harmonic expansions given by equations (1)–(4) and the Fourier expansions for the permittivity and its inverse given by (13) and (14) have to be truncated. The truncation extent is decided by the accuracy required by our problem. One nonpropagating order and some primary terms corresponding to all the propagating orders in each direction should be retained for reasonable accuracy of our results. In our calculations, we find that the reflectivity of the grating is almost constant when the indices m and n are larger than 5, and p and q are larger than 9, if other parameters of the grating structure are kept constant at the same time. Thus to reduce the dimension of the matrix in the computation and improve the computational speed, we take $m = n = 5$ and $p = q = 9$. In this case, the number of terms is sufficient to ensure accuracy to five decimal places for the result. Conservation of energy is also achieved to within 1 part in 10^9.

We consider the grating structures obtained by etching the columned grid pattern onto a glass and a silicon substrate using ion beam etching, respectively. Other basic parameters are $\lambda = 1.533$ μm, $\epsilon^{\mathrm{I}} = 1$ and $\epsilon^{\mathrm{III}} = 2.25$ for the glass grating and $\lambda = 10$ μm, $\epsilon^{\mathrm{I}} = 1$ and $\epsilon^{\mathrm{III}} = 9$ for the grating with a silicon substrate, respectively. The angles that specify the propagation direction of the incident wave and the polarization vector are shown in figures 1 and 2. For simplicity, we also take $T_x = T_y = T$, which makes the spatial periods along both x and y directions equal. In the following diagrams of our results the vertical axes of all plots give the reflectivity of the grating. Our primary interest is to analyse the antireflection properties of the columned grid gratings with various given parameters.

In figures 4 and 5, the reflectivity curves at normal incidence for different column diameters with different substrates are plotted. We find that the reflectivity dips to zero for certain values of the diameter. By varying the diameters of the columns from zero to a grating spatial period T, it is found that the minimum reflectivity is obtained when the column diameter is 0.79 T for the glass grating and 0.71 T for the silicon grating.

In figures 6 and 7, the reflectivity curves at normal incidence for different column heights are presented. For the same arrangement as in figures 4 and 5, the reflectivity reaches a minimum for the grating with a glass substrate when the column height is 0.21λ or 0.62λ. Figure 7 predicts a lowest reflectivity for the silicon grating when the grating depth is 0.16λ. Beyond that point, the reflectivity has an oscillatory behaviour but is always larger than its minimum value.

Figures 8 and 9 show the relation between reflectivity and grating spatial period. In both figures, the grating depths and diameters of the column array correspond to those of figures 4 to 7. It is shown that the reflectivity increases as the period in

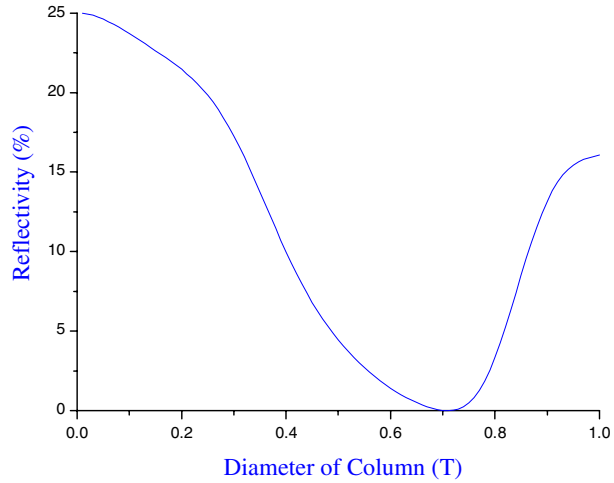

Figure 5. Relation between reflectivity and column diameter for a silicon substrate, with parameters: $T = 0.69\lambda$; $h = 0.16\lambda$; $\Psi = 90^\circ$; $\alpha = \delta = 0^\circ$; $n_i = 1.0$; $n_s = 3.0$.

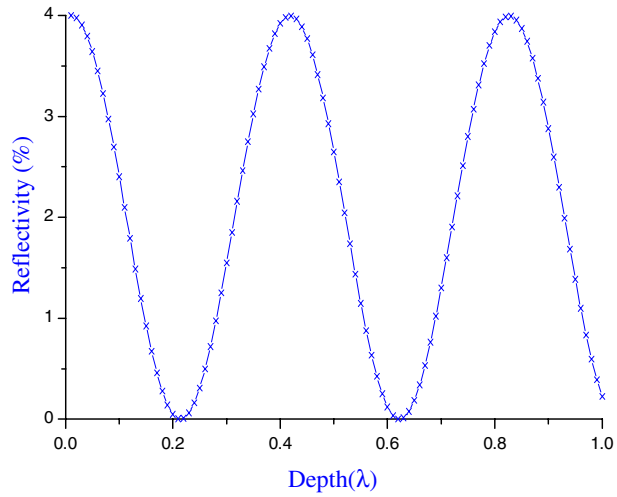

Figure 6. Relation between reflectivity and the depth of a glass grating, with parameters: $T = 0.1\lambda$; $R = 0.79$ T; $\Psi = 90^\circ$; $\alpha = \delta = 0^\circ$; $n_i = 1.0$; $n_s = 1.5$.

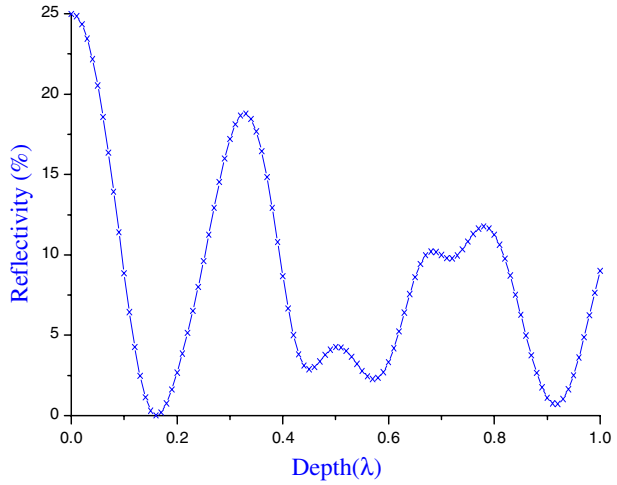

Figure 7. Relation between reflectivity and the depth of a silicon grating, with parameters: $T = 0.69\lambda$; $R = 0.71$ T; $\Psi = 90^\circ$; $\alpha = \delta = 0^\circ$; $n_i = 1.0$; $n_s = 3.0$.

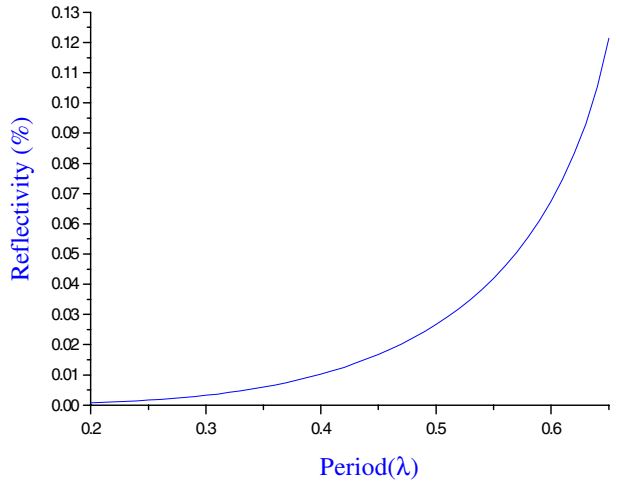

Figure 8. Relation between reflectivity and spatial period for a glass grating, with parameters: $R = 0.79$ T; $h = 0.205\lambda$; $\Psi = 90^\circ$; $\alpha = \delta = 0^\circ$; $n_i = 1.0$; $n_s = 1.5$.

figure 8, but for the silicon grating in figure 9, the reflectivity has a minimum at a particular value of the grating period.

The relation of the reflectivity versus incident angle is shown in figures 10 and 11. It is obvious that the reflectivity increases rapidly after the incident angle exceeds a certain value. In figure 10, the reflectivity of the glass grating is less than 0.5% if the angle is smaller than 30°, but increases rapidly after the incident angle exceeds 25°. Thus we find that the glass grating can reduce reflection over a broad field of incidence. If it is desired to have antireflection over a broader field of incidence, a more complicated interface structure grating is necessary, such as a 2D multilevel grating. We find from figure 11 that the silicon grating can achieve low reflectance (less than 5%) over a broader field of incidence ($\theta_{\mathrm{FOV}} > 130^\circ$). Although the reflectivity of this grating with the special parameters of figure 11 is appreciably larger than that of Eric's tapered grating structures [21], its field of view is wider and fabrication is easier, so this grating can satisfy the needs of lower reflectivity and broader field of view.

Figure 12 shows the reflectivity curves for the glass grating in the visible region at normal incidence. The computation program was designed for a centre wavelength of 550 nm, and the parameters used are: $T = 0.1\lambda$, $R = 0.79$ T, $h = 0.205\lambda_0$. We find this grating can be designed to cover almost the whole visible light band. Figure 13 shows the reflection curves for the silicon grating in the far-infrared region for normal incidence. Compared with the result of Eric's rectangular grid grating [20], lower reflectivity in this waveband is obtained. From both figures, the gratings reduce reflections only at a particular wavelength. If it is required to reduce the reflections over a broad band of frequencies, it will be necessary to construct a more complicated interference structure.

The relations of the reflectivity versus azimuth angle and polarization angle for the glass grating are shown in figure 14. It can be seen that when the azimuth and polarization angles of the incident wave are varied from 0° to 90° there is hardly any change in the reflectivity. The programs ensure accuracy of the calculation to ten decimal places in both cases, so the gratings can reduce reflection from unpolarized light.

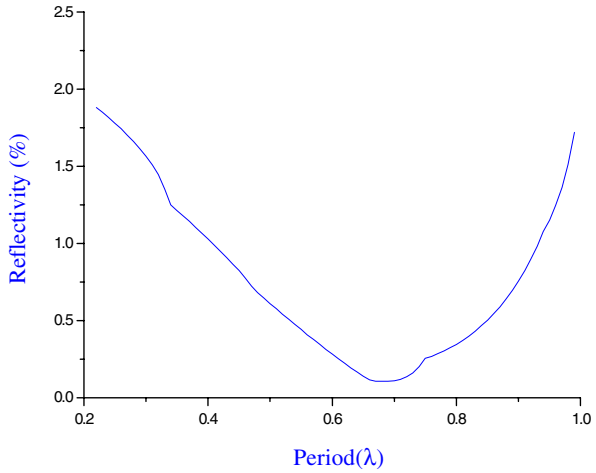

Figure 9. Relation between reflectivity and spatial period for a silicon grating, with parameters: $R = 0.70$ T; $h = 0.17\lambda$; $\Psi = 90°$; $\alpha = \delta = 0°$ $n_i = 1.0$; $n_s = 3.0$.

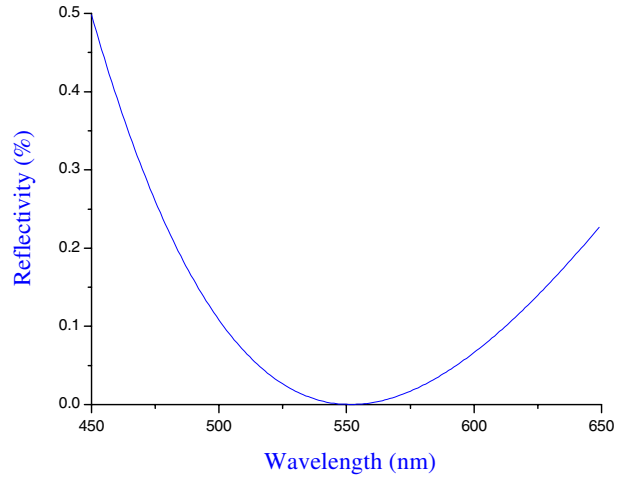

Figure 12. Diagram of reflectivity in the visible wave band for a glass grating, with parameters: $\lambda_0 = 550$ nm; $T = 0.1\lambda_0$; $R = 0.79$ T $h = 0.205\lambda_0$; $\alpha = \phi = 0°$; $\Psi = 90°$; $n_i = 1.0$; $n_s = 1.5$.

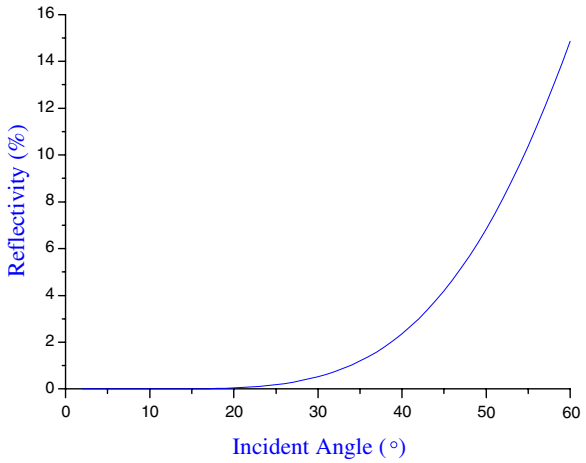

Figure 10. Relation between reflectivity and incident angle for a glass grating, with parameters: $T = 0.1\lambda$; $R = 0.79$ T $h = 0.21\lambda$; $\Psi = 90°$; $\delta = 0°$; $n_i = 1.0$; $n_s = 1.5$

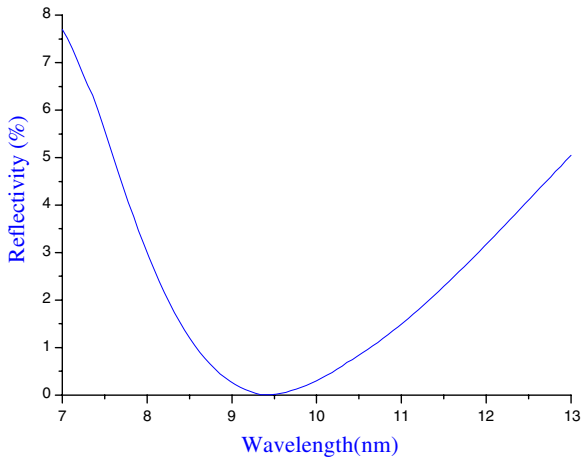

Figure 13. Diagram of reflectivity in the far infrared wave band for a silicon grating, with parameters: $\lambda_0 = 10$ μm; $T = 0.69\lambda_0$; $R = 0.79$ T $h = 0.15\lambda_0$; $\alpha = \phi = 0°$; $\Psi = 90°$; $n_i = 1.0$; $n_s = 3.0$.

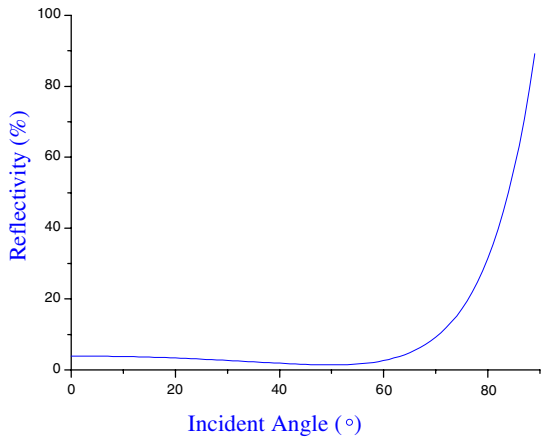

Figure 11. Relation between reflectivity and incident angle for a silicon grating, with parameters: $T = 0.33\lambda$; $R = 0.71$ T $h = 0.19\lambda$; $\Psi = 90°$; $\delta = 0°$; $n_i = 1.0$; $n_s = 3.0$.

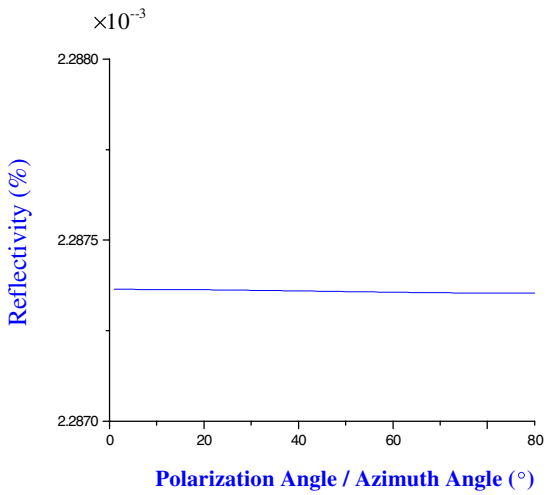

Figure 14. Relation between reflectivity and polarization angle or azimuth angle for a glass grating, with parameters: $T = 0.1\lambda$; $R = 0.79$ T; $h = 0.205\lambda$; $\Psi = 90°$; $\alpha = 0°$; $n_i = 1.0$; $n_s = 1.5$.

5. Summary and conclusions

In this paper, the algorithms of coupled-wave analysis are reviewed and the results of our computer simulation for the columned grid grating are presented.

We find that glass gratings can be designed to cover almost the whole visible light band with a broader field of incidence. It is shown that these gratings are capable of reducing reflections from unpolarized light. Compared with the results published by Eric [20, 21], we also find that the maximum normalized transmittance in the far infrared of a columned grid grating with a silicon substrate is larger than that of a rectangular grating, and also can achieve low reflectance over a broad field of view like the tapered grating structure, but the fabrication of the columned grating is simpler than that of the tapered grating structure.

Through computer simulation we have obtained relationships between the reflection and grating parameters. We find that the glass grating reflectivity is approximately zero for special parameter values, i.e. $T = 0.2\lambda$, $h = 0.21\lambda$ and $\alpha < 25^\circ$. This should be very useful in the design of certain novel optical systems.

Our result always satisfies energy conservation, and fortunately the numerical instability problem of reference [19] and the convergence problem of references [18–20] do not emerge in our calculations for this subwavelength structure. By using Matlab and Visual C++ together, our programs are easily implemented with greater economy in computing time and storage, but the full range of applicability of our programs is yet to be explored.

Acknowledgment

We gratefully acknowledge support from the National Natural Science Foundation of China.

References

[1] Bräuer R and Bryngdahl O 1993 *Opt. Commun.* **100** 1–5
[2] Vincent P 1978 *Opt. Commun.* **26** 293–6
[3] Han S T, Tsao Y-L, Walser R M and Becker M F 1992 *Appl. Opt.* **31** 2343–52
[4] Wilson S J and Hutley M C 1982 *Opc. Acta* **29** 993–1009
[5] Ono Y, Kimura Y, Ohta Y and Nishida M 1987 *Appl. Opt.* **26** 1142–6
[6] Norman S L and Sinch M P 1975 *Appl. Opt.* **4** 818–20
[7] Petit R and Tayeb G 1987 *Proc. SPIE* **815** 2–10
[8] Moharam M G and Gaylord T K 1982 *J. Opt. Soc. Am.* **72** 1385–92
[9] Press W H, Flannery B P, Teukolsky S A and Vetterling W T 1988 *Numerical Recipes* (Cambridge: Cambridge University Press)
[10] Cowan J J 1985 *Proc. SPIE* **523** 251–9
[11] Nurns J R 1985 *Proc. SPIE* **523** 7–14
[12] Gaylord T K and Moharam M G 1985 *Proc. IEEE* **73** 894–937
[13] Moharam M G 1988 *Proc. SPIE* **883** 8–11
[14] Knop K 1978 *J. Opt. Soc. Am.* **68** 1206–10
[15] Li L 1996 *J. Opt. Soc. Am.* A **13** 1870–76
[16] Russell P St J 1984 *J. Opt. Soc. Am.* A **13** 293–9
[17] Moharam M G and Gaylord T K 1983 *J. Opt. Soc. Am.* **73** 1105–12
[18] Peng S and Michael M G 1995 *J. Opt. Soc. Am.* **12** 1089–96
[19] Moharam M G, Grann E B and Pommet D A 1995 *J. Opt. Soc. Am.* **12** 1068–76
[20] Grann E B, Moharam M G and Pommet D A 1995 *J. Opt. Soc. Am.* **12** 333–9
[21] Grann E B, Moharam M G and Pommet D A 1994 *J. Opt. Soc. Am.* **11** 2695–703